scientific reports

Check for updates

OPEN

Dual-responsive bis-Schiff base fluorescent probe for simultaneous detection of Zn^{2+} and HClO in environmental monitoring and information encryption

Fan Yang[1], Yinglong Ma[1], Hanxun Zou[1], Yang Liu[2], Xiaopei Li[2]✉ & Jing Huang[1]✉

The dysregulation of zinc ions (Zn^{2+}) and hypochlorous acid (HClO) poses significant threats to ecological systems and human health. Consequently, the development of robust analytical tools for the detection of these ions is imperative. While numerous fluorescent probes exist for individual analytes, the creation of single-molecule platforms for dual detection remains a formidable challenge. In this study, we reported a novel bis-Schiff base fluorescent probe (P-B) for the simultaneous and distinct detection of Zn^{2+} and HClO. In the presence of Zn^{2+}, the probe displays a substantial "turn-on" fluorescence response at 520 nm with high selectivity, rapid response time (< 60 s) and exceptionally low detection limit of 17.50 nM. In contrast, P-B functions as a "turn-off" sensor for HClO, enabling selective detection with a limit of 0.24 μM. The practical utility of P-B was successfully validated in real-world applications. The instrument was utilized for the on-site, visual screening of Zn^{2+} contamination in soil samples and for quantitative detection in environmental water. Furthermore, the unique "invisible-to-visible" fluorescence transformation of the compound upon binding with Zn^{2+} was ingeniously leveraged to develop an advanced information encryption system. This simple, robust, versatile molecular tool holds significant promise for environmental monitoring and information security applications.

Keywords Fluorescent probe, Dual-responsive, Schiff base, Zinc ion, Hypochlorous acid

Zinc ions (Zn^{2+}), the second most abundant transition metal ions in biological systems after iron, are indispensable for a multitude of physiological functions. These elements serve as critical cofactors for numerous enzymes, play a structural role in transcription factors, and are integral to processes such as immune defense, signal transduction, cell metabolism, and gene expression regulation. Consequently, they play a pivotal role in maintaining organismal homeostasis[1–5]. However, the dysregulation of Zn^{2+} homeostasis has been implicated in severe pathological conditions. An excessive accumulation of Zn^{2+} has been demonstrated to induce cellular toxicity, metabolic dysfunction, and contribute to the progression of various diseases, including diabetes, cancer, and Alzheimer's disease[6–10]. Concurrently, hypochlorous acid (HClO), a primary reactive oxygen species (ROS), functions as a pivotal mediator within the innate immune system, contributing to both host defense and inflammatory signaling[11–13]. Its potent oxidizing and antimicrobial properties have also led to its widespread application as a disinfectant and preservative[14–17]. However, elevated levels of HClO can induce oxidative damage to cellular and tissue structures, resulting in inflammation, arthritis, and cardiovascular diseases. Furthermore, its application in water treatment can yield carcinogenic byproducts[18–22]. The dual roles of both Zn^{2+} and HClO underscore the critical need for robust analytical tools capable of their sensitive and selective detection in both environmental and biological contexts.

Conventional analytical techniques for monitoring environmental pollutants, such as spectrophotometry, electroanalysis, and chromatography, have been established for the detection of these species[23–29]. While these methods have proven to be effective, they often require sophisticated instrumentation, meticulous sample

[1]Fujian Provincial Key Laboratory of Ecological Impacts and Treatment Technologies for Emerging Contaminants, Key Laboratory of Ecological Environment and Information Atlas (Fujian Provincial University), College of Environmental and Biological Engineering, Putian University, Putian 351100, Fujian, China. [2]Baotou Research Institute of Rare Earths, Baotou 014030, Inner Mongolia, China. ✉email: xplee@brire.com; jinghuang@ptu.edu.cn

preparation, and operation by specialized personnel, thereby limiting their utility for rapid, on-site, or real-time applications. Conversely, fluorescent probes have emerged as a compelling alternative, offering distinct advantages, including high sensitivity and selectivity, rapid response kinetics, operational simplicity, cost-effectiveness, and suitability for bioimaging with high spatiotemporal resolution[30–41]. Despite the development of numerous fluorescent probes for either Zn^{2+} or HClO[42–46], the design of simple, single-molecule platforms capable of simultaneously detecting both analytes remains a significant challenge. The development of such dual-responsive probes is imperative for enhancing environmental monitoring and elucidating complex biological processes in which these species may coexist.

In the realm of sensor design, Schiff base derivatives have emerged as a particularly versatile class of molecular scaffolds, distinguished by their unique imine (-N = CR-) moiety. These derivatives have demonstrated remarkable efficacy in the development of fluorescent probes that target metal ions and reactive oxygen species (ROS)[47–49]. The nitrogen atom of the imine group provides a strong coordination site for metal ions, enabling Schiff bases to function as excellent polydentate chelating agents that form stable complexes. These complexes often trigger a "turn-on" fluorescence response via mechanisms like Chelation-Enhanced Fluorescence (CHEF)[50–55]. Additionally, the imine bond is vulnerable to oxidative cleavage by potent oxidants, such as HClO, under mild conditions. This specific chemical transformation can be harnessed as a distinct sensing mechanism, leading to a secondary, measurable change in the probe's fluorescence output[56–58]. This distinctive dual reactivity renders Schiff bases an optimal medium for constructing multi-analyte sensors.

In this study, we present the rational design and synthesis of P-B, a novel bis-Schiff base fluorescent probe. The probe was prepared through a straightforward Duff reaction and subsequent condensation involving 4-ethoxyphenol and hexamethylenetetramine. This probe exhibits remarkable performance, facilitating the efficient and selective detection of both Zn^{2+} and HClO through distinct and substantial fluorescence changes. The practical utility of the P-B probe is underscored by its successful application in the on-site screening of Zn^{2+} contamination in soil samples. The probe has also been leveraged in the development of an advanced information encryption system. This work presents a robust and versatile molecular tool with promising applications in environmental science and information security.

Experimental

Materials and characterization

All solvents and chemicals were procured from Shanghai Titan Scientific Co., Ltd. and utilized without additional purification. The water samples were collected from Fangming Lake at Putian University and from tap water in the laboratory. The soil samples were obtained from the arable layer (0–20 cm) from a sandy field Taihu Village, Lingchuan Town, Chengxiang District, Putian City, and Zn^{2+} solution was sprayed onto the soil to simulate contamination (Specific details see the Supporting Information).

The ^{1}H and ^{13}C NMR spectra were recorded on a Bruker AVANCE III-400 NMR spectrometer using tetramethylsilane (TMS) as the internal reference standard. The high-resolution mass spectrum (HRMS) was measured using an Agilent 6540 TOF. The FT-IR spectra were obtained between 4000 and 400 cm^{-1} with a Bruker TENSON27 FT-IR spectrometer. The UV-Vis measurements were operated at SHIMADZU UV-2550 spectrophotometer. The fluorescence emission spectra were measured using a Carry Eclipse fluorescence spectrometer. The photoluminescence quantum yield and lifetime were performed by an Edinburg FLS1000 photoluminescence spectrometer.

Synthesis of bis-Schiff base fluorescent probe P-B

As illustrated in Fig. 1, the Duff reaction was employed to introduce aldehyde groups at the ortho position of the phenolic hydroxyl groups, thereby yielding compound P-A. Subsequently, compound P-A was subjected to a condensation reaction with 2-hydrazinylbenzothiazole, yielding the bis-Schiff base fluorescent probe P-B.

Synthesis of compound P-A. A solution of 4-methoxyphenol (0.50 g, 4.0 mmol) and hexamethylenetetramine (1.13 g, 8 mmol) in trifluoroacetic acid (TFA, 20 mL) was prepared. The mixture was subjected to heating at a

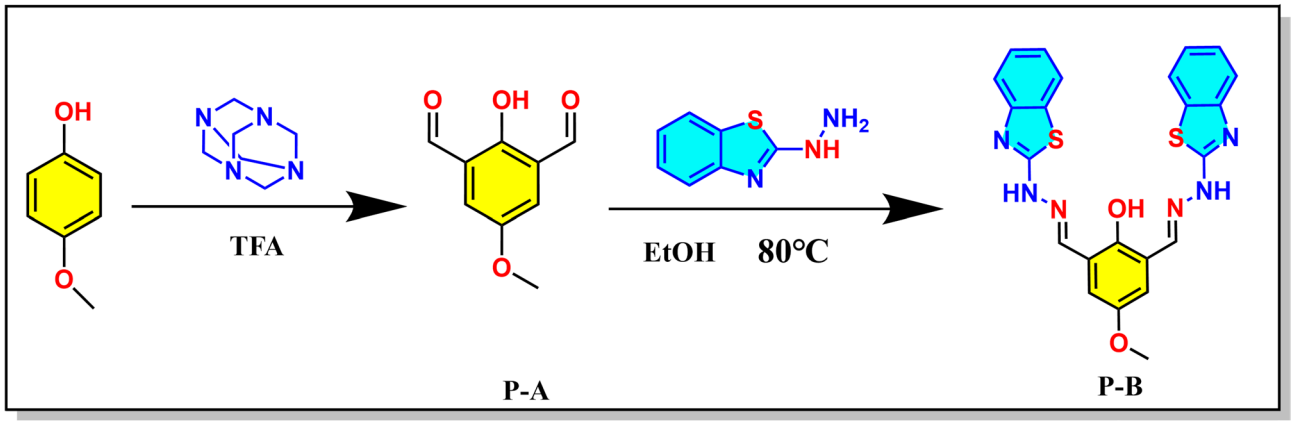

Fig. 1. Synthesis process for the probe P-B.

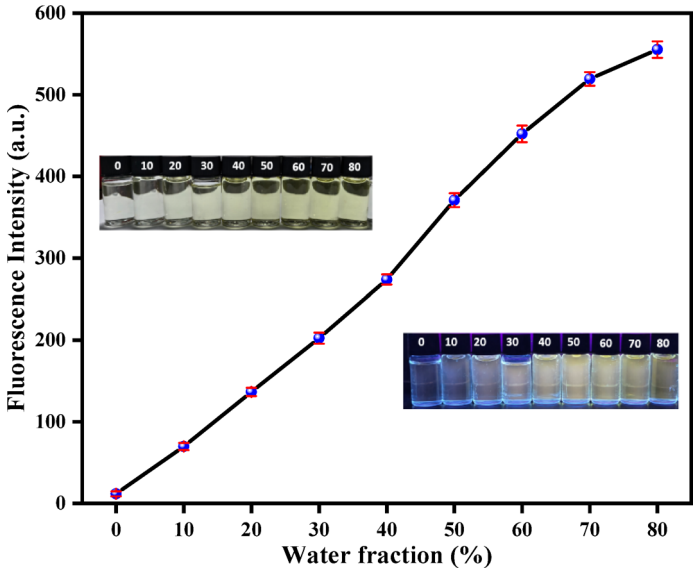

Fig. 2. Point-line plot of the fluorescence intensity at 550 nm in different water content (v%) solution. Inset: Photographs of P-B in different water content (v%) solution under daylight or 365 nm UV light. (THF/H_2O, λ_{ex} = 400 nm, slits: 5 nm/5 nm).

temperature of 70 °C for a period of 4 h. Subsequent to the completion of the reaction and subsequent cooling to room temperature, 30 milliliters of ice water was added, followed by the addition of sodium bicarbonate to adjust the pH to neutral. Subsequently, the mixture was extracted with ethyl acetate (EA). The amalgamation of organic layers underwent desiccation over anhydrous $MgSO_4$, followed by evaporation under reduced pressure. The residue was subjected to a purification process involving column chromatography on a silica gel column, eluting with a mixture of CH_2Cl_2 and MeOH (20:1). This procedure resulted in the isolation of compound P-A, which was characterized as a pale-yellow solid (0.42 g, 26% yield). The ^{1}H NMR spectrum (DMSO-*d*6, 400 MHz) was recorded as follows: 11.06 (s, 1H), 10.24 (s, 2 H), 7.60 (s, 2 H), and 3.82 (s, 3 H). The ^{13}C NMR spectrum (DMSO-*d*6, 100 MHz) exhibited the following signal peaks (ppm): 192.18, 156.93, 152.62, 124.80, 121.85, and 56.39. The HRMS (ESI) calculation for $C_9H_9O_4$ $[M+H]^+$ yielded a molecular weight of 181.0501, while the experimental value obtained was 181.0507, indicating a slight discrepancy.

Synthesis of compound P-B. A solution of 2-hydrazinobenzothiazole (0.66 g, 0.4 mmol) in ethanol (15 mL) was added dropwise to an ethanol solution (15 mL) of P-A (0.36 g, 0.2 mmol). Subsequently, the mixture solution was stirred and subjected to reflux for a period of 6 h at a temperature of 80 °C. Subsequent to the completion of the reaction and subsequent cooling to room temperature, the solution was evaporated to 4 mL under reduced pressure and recrystallized in ethanol. Following the vacuum drying process, compound P-B was obtained in the form of a yellow solid. (0.75 g, 74% yield). The ^{1}H NMR spectrum (DMSO-*d*6, 400 MHz) was recorded as follows: 12.39 (s, 2 H), 11.29 (s, 1H), 8.53 (s, 2 H), 7.80 (d, J = 8 Hz, 2 H), 7.33 (m, 6 H), 7.15 (t, J = 8 Hz, 2 H), and 3.84 (s, 3 H). The HRMS (ESI) was utilized to calculate the molecular weight of $C_{23}H_{19}N_6O_2S_2$ $[M+H]^+$ at 475.1011, which was subsequently found to be 475.1032.

Optical studies process

A stock solution of probe P-B (100 μM) was prepared in tetrahydrofuran (THF) for aggregation-induced emission (AIE) study and in dimethyl sulfoxide (DMSO) for investigation of Zn^{2+}/hydrochloric acid (HClO) responsiveness. A stock solution of metal ions (100 μM) was prepared, including (Fe^{3+}, Ca^{2+}, K^+, Mn^{2+}, Hg^{2+}, Co^{2+}, Ni^{2+}, Mg^{2+}, Li^+, Zn^{2+}, Pb^{2+}, Cd^{2+}, Cu^{2+}, Al^{3+}, Eu^{3+}, Tb^{3+} and Cr^{3+}). This solution was prepared in pure water for Zn^{2+}-responsive investigation. A stock solution of other analytes (1 mM) was prepared, including Cl^-, CH_3COO^-, NO_2^-, NO_3^-, SO_4^{2-}, SO_3^{2-}, and HClO, in a pure water solution for HClO-responsive investigation. Unless otherwise specified, the parameters of the fluorescence spectrophotometer were set as follows: photomultiplier tube voltage of 600 V, excitation slit width of 5 nm, emission slit width of 5 nm, excitation wavelength of 400 nm, and fluorescence emission spectra were recorded in the wavelength range of 420–700 nm. The detailed operation steps are delineated in the Supporting Information. Tests with error bars were all based on three parallel experiments.

Results and discussion

Photophysical properties of probe P-B

The photophysical properties of P-B were systematically examined in DMSO/H_2O (7:3) with the corresponding UV-vis and fluorescence spectra displayed in Supplementary Fig. 3. P-B showed maximum absorption wavelength at 338 nm and maximum emission wavelength at about 500 nm. Notably, P-B exhibited a large Stokes shift of 162 nm, which could avoid self-absorption and interference in fluorescence measurements. To investigate the AIE behaviors of P-B, the fluorescent emission spectra were carried out in THF/H_2O mixed solution with different

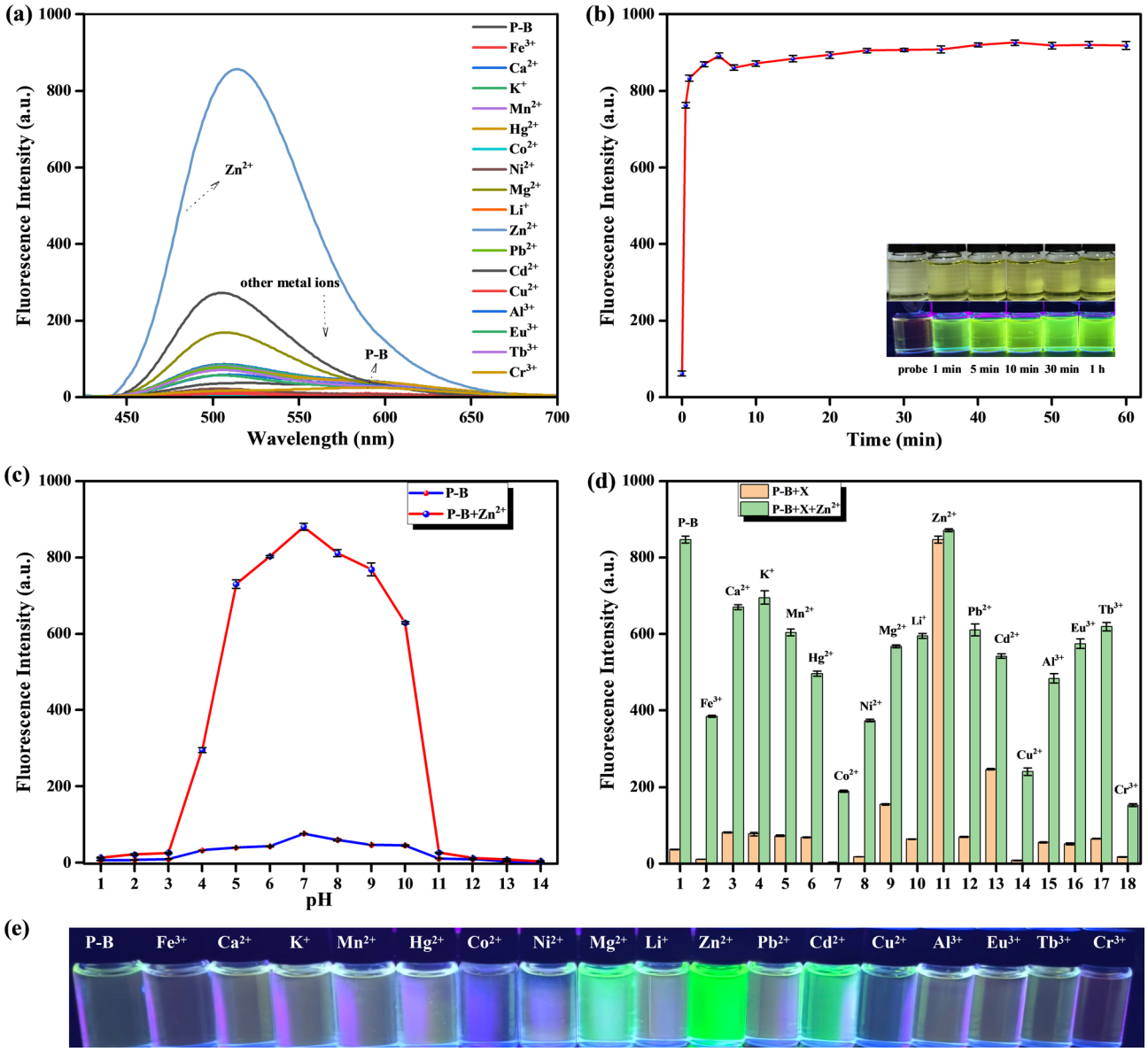

Fig. 3. (**a**) Fluorescence spectra of P-B in the presence of different metal ions. (**b**) Point-line plot of the fluorescence intensity at 520 nm versus incubation time of the P-B with Zn^{2+}. Inset: Photographs of the P-B with Zn^{2+} in different incubation time under sunlight or 365 nm UV light. (**c**) Point-line plot of the fluorescence intensity at 520 nm in different pH of P-B and P-B + Zn^{2+}. (**d**) Fluorescence response of adding Zn^{2+} to the solution containing P-B and various ions (pink bars are the solution of P-B with various cations, green bars are the solution after adding Zn^{2+}. 1-P-B, 2-Fe^{3+},3-Ca^{2+}, 4-K^{+}, 5-Mn^{2+},6-Hg^{2+}, 7-Co^{2+}, 8-Ni^{2+},9-Mg^{2+},10-Li^{+}, 11-Zn^{2+},12-Pb^{2+}, 13-Cd^{2+},14-Cu^{2+}, 15-Al^{3+}, 16-Eu^{3+}, 17-Tb^{3+}, 18-Cr^{3+}). (e) Photographs of the P-B with Zn^{2+} in different incubation time under 365 nm UV light. (DMSO/H_2O = 7/3, v/v, λ_{ex} = 400 nm, slits: 5 nm/5 nm).

water fraction. P-B exhibited good solubility in THF, yet it was hardly to dissolve in water. Therefore, it showed a tendency to aggregate in THF/H_2O mixture with high water fraction. As shown in Fig. 2, with the increase of water fraction, the fluorescence intensity (550 nm) was enhanced and the P-B solution emitted bright yellowish green fluorescence under 365 nm UV lamp. The fluorescence intensity at 550 nm reached the maximum when *fw* = 80%, resulting in a ca. 65-fold increment compared to the initial intensity (Supplementary Fig. 4). The change of fluorescent emission with the water fraction due to the restriction of C-N rotation caused by the aggregation of P-B, which manifested as aggregation-induced emission characteristics[59]. However, when the water volume fraction (*fw*) exceeds 80%, the emission intensity at 550 nm began to reduce evidently, which might be due to the fact that the aggregates of P-B rapidly undergo random agglomeration to form excimers, whose energy is more likely to dissipate through non-radiative transitions, ultimately leading to fluorescence weakening.

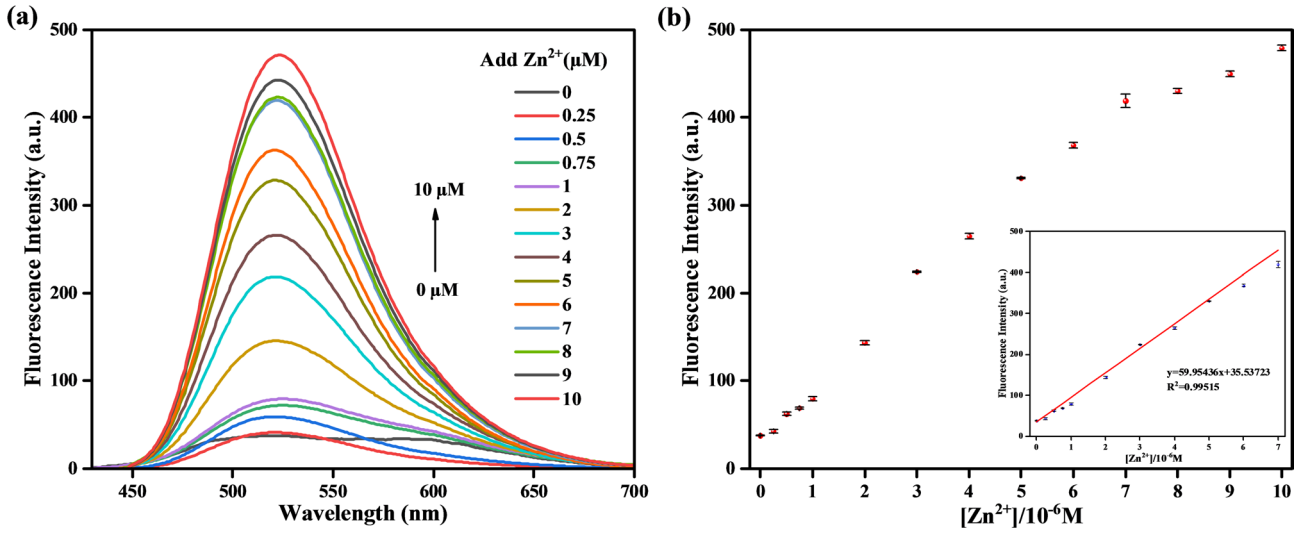

Fig. 4. (**a**) The fluorescence spectra of P-B with different concentrations of Zn^{2+} (0–10 μM). (**b**) Relationship between concentration of Zn^{2+} and fluorescence intensity at 520 nm. (DMSO/H_2O = 7/3, v/v, λ_{ex} = 400 nm, slits: 5 nm/5 nm).

Fluorescence response of P-B to Zn^{2+}

Firstly, the selectivity of the probe P-B in a range of metal ions (Fe^{3+}, Ca^{2+}, K^{+}, Mn^{2+}, Hg^{2+}, Co^{2+}, Ni^{2+}, Mg^{2+}, Li^{+}, Zn^{2+}, Pb^{2+}, Cd^{2+}, Cu^{2+}, Al^{3+}, Eu^{3+}, Tb^{3+}, Cr^{3+}) was investigated. As depicted in Fig. 3a, upon the addition of the above-mentioned metal ions to the P-B solution, the fluorescence spectra of most ions remained unaffected. Although the addition of Mg^{2+} and Cd^{2+} led to a certain increase in the fluorescence intensity, the degree of this increase was far lower than that caused by the addition of Zn^{2+}. Specifically, after introducing Zn^{2+}, the fluorescence intensity increased by nearly 20 times. Figure 3e exhibited that the strong green fluorescence appeared when Zn^{2+} was present under 365 nm ultraviolet light which could be easily observed through the naked eyes, enabling clear distinction with the addition of other metal ions. These results indicated that P-B exhibits high selectivity for Zn^{2+}, whether through spectrogram analysis or visual observation.

Furthermore, to evaluate the sensitivity and stability of P-B, we monitored the time-dependent fluorescence intensity of the P-B solution following the addition of Zn^{2+}. As shown in Supplementary Fig. 5 and Fig. 3b, upon addition of Zn^{2+}, the fluorescence at 520 nm increased rapidly and reached equilibrium within 60 s. Meanwhile, the fluorescence intensity maintained stable at least 60 min in the process of recognizing Zn^{2+}. Besides, the photographs in the inset of Fig. 3b reveal that the P-B solution immediately emits green fluorescence with the addition of Zn^{2+}, which can persist for 60 min. The above results confirm that probe P-B exhibits excellent sensitivity and stability in the detection of Zn^{2+}.

Usually, the pH value of a real detection environment could affect significantly the fluorescence behavior of chemosensors, therefore the effect of pH was also investigated (Supplementary Fig. 6 and Fig. 3c). There was no significant change in fluorescence intensity at 520 nm of probe P-B over the range pH 1–14. In the presence of Zn^{2+}, the fluorescence intensity at 520 nm declined rapidly when pH values were < 5, this decline can be attributed to decomposition of P-B in acidic conditions. Fluorescence intensity of P-B with Zn^{2+} increased to a maximum value and kept relatively stable at pH 6–8, but fluorescence decreased rapidly at pH > 9. This decrease could be due to competition between P-B and OH ions for Zn^{2+}, and increasing hydroxide forms of Zn^{2+}. Therefore, the applicable pH range for this probe to detect Zn^{2+} should be in the range 6–8, which is consistent with the physiological pH range and favorable for its biological applications in living cells and in vitro.

The anti-interference of probe P-B plays a vital role in the accurate detection of Zn^{2+} in complicated real environments. To explore the anti-interference ability of the probe P-B in detecting Zn^{2+}, 14 interfering cations were added to the probe P-B solution. As shown in Fig. 3d, after adding the interfering cation, the fluorescence intensity of the system changed slightly, and after adding Zn^{2+} to each of the above solutions, the fluorescence intensity of the system showed a significant increase. Overall, through these assays, probe P-B demonstrated good anti-interference ability to Zn^{2+} detection and might be applied as a useful fluorescent chemosensor for Zn^{2+} in complicated detection environments.

To evaluate the sensing ability of the probe P-B for Zn^{2+}, the fluorescence titration experiments were performed and the fluorescence response of P-B to different concentrations of Zn^{2+} were shown in Fig. 4. As the concentration of Zn^{2+} (0–10 μM) increased, the fluorescence at 520 nm gradually enhanced. A good linear relationship was obtained in the Zn^{2+} concentration range of 0–7 μM. The absolute slope of the linear relationship between the fluorescence intensity at 520 nm and Zn^{2+} (0–7 μM) was found to be 59.95436. Additionally, the standard deviation of the fluorescence intensity at 520 nm for the 8 blank samples was calculated to be 0.34981 (Supplementary Fig. 7 and Supplementary Table 2). Using the formula 3σ/k, the calculated limit of detection (LOD) was 17.50 nM, which is lower than most of the values reported for Zn^{2+} probes (Supplementary Table 3). As determined from the Supplementary Fig. 1, the binding constant of P-B with Zn^{2+} was $6.285 \times 10^4\ M^{-1}$.

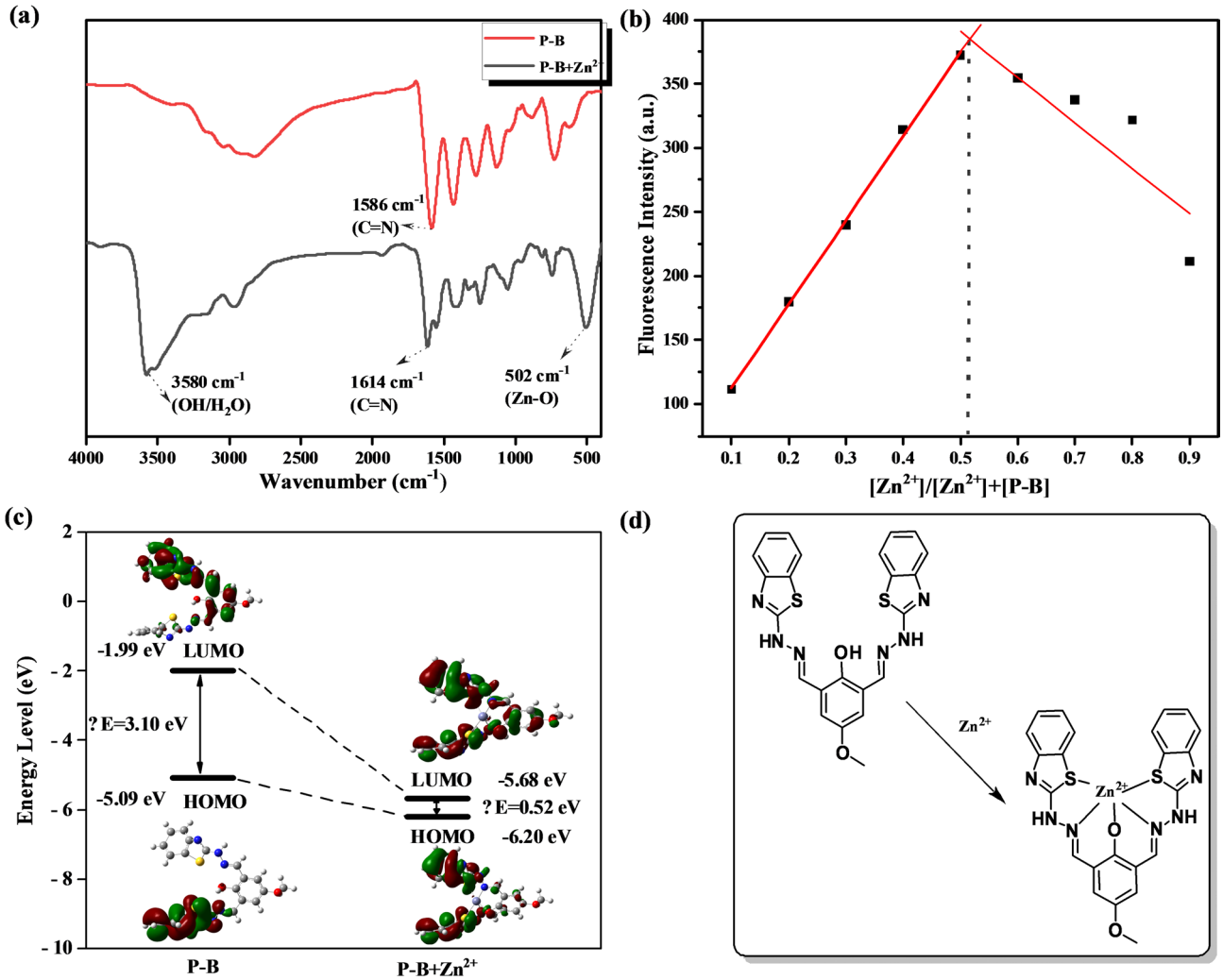

Fig. 5. (**a**) The FTIR spectra of P-B and P-B + Zn^{2+}. (**b**) Job's plot for the different ratio of P-B and Zn^{2+}. (DMSO/H_2O = 7/3, v/v, λ_{ex} = 400 nm, slits: 5 nm/5 nm). (**c**) Optimized molecular structures and corresponding orbital electron distribution of P-b with or without Zn^{2+}. (d) Recognition mechanism of the probe for Zn^{2+}.

To verify the binding mode of P-B and Zn^{2+}, the FTIR spectra was employed firstly. As shown in Fig. 5a, in the spectrum of P-B, the C = N band was observed at 1586 cm^{-1}. With the addition of Zn^{2+}, the band of C = N shifted to 1614 cm^{-1} which was ascribed to the enhanced coordination between Zn^{2+} and the N atoms in P-B. Additionally, a distinct absorption peak attributed to the Zn-O bond appears at 502 cm^{-1}, which can be ascribed to the coordination of Zn^{2+} with the oxygen atoms in probe P-B. The emergence of the Zn-O absorption band, combined with the shifts in the C = N bands, jointly confirm the synergistic coordination between probe P-B and Zn^{2+}. Besides, the high-resolution mass spectrum of P-B + Zn^{2+} (Supplementary Fig. 17) was performed. The molecular weight of generation complex ($C_{23}H_{17}N_6O_2NaS_2Zn$) at 560.0053 corresponded to the $[P\text{-}B + Zn + Na - H]^+$ complex. This result further confirmed the formation of Zn-O bond and the 1:1 stoichiometric ratio between probe and Zn^{2+}. To further confirm the stoichiometry of P-B and Zn^{2+}, the coordination of Zn^{2+} was analyzed and determined using the Job's Plot method. As shown in Fig. 5b and Supplementary Fig. 8, when the total concentration of the probe and Zn^{2+} was kept constant, the fluorescence intensity increased gradually as the proportion of Zn^{2+} rose. When $[Zn^{2+}]/([Zn^{2+}] + [P\text{-}B]) = 0.50$, the fluorescence intensity of the mixed solution reached a maximum, indicating a 1:1 coordination ratio between the probe and Zn^{2+}.

To evaluate the impact of metal coordination on the photophysical properties of the probe, the fluorescence lifetimes of P-B and P-B with Zn^{2+} were measured on excitation of samples at 400 nm (Supplementary Fig. 9). The observed florescence decays fit well with the exponential decay profile, which was supported by the goodness-of fit ($\chi 2$) data in the regression analyses. In DMSO/H_2O (7:3), P-B exhibited a bi-exponential fluorescence decay profile with an average lifetime of 3.26 ns. Upon addition of Zn^{2+}, it maintained a bi-exponential decay characteristic while showing a more than 1.65-fold increase in lifetime, reaching 5.40 ns. Furthermore, the photoluminescence quantum yield of the P-B with Zn^{2+} (Φ = 30.2%) was 2.9-fold higher than that of the uncoordinated P-B (Φ = 10.5%) in DMSO/H_2O (7:3) solution. This elevation in quantum

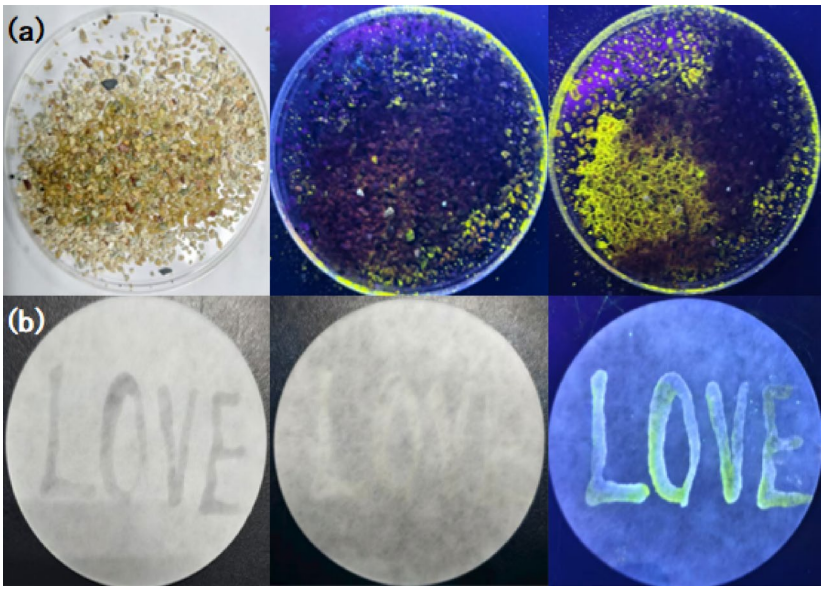

Fig. 6. (**a**) Daylight image of soil sample (left), fluorescence images under 365 nm UV light after spraying a small amount (middle) and an excess of probe solution P-B (right). (**b**) "LOVE" written with Zn^{2+} solution on filter paper (left), its daylight image after air-drying (middle), and fluorescence image under 365 nm UV light after spraying with probe solution P-B (right).

yield further corroborated the fluorescence lifetime data, confirming that metal coordination enhances the photophysical properties of the probe by enabling more efficient emission. Density functional theory (DFT) calculations further demonstrated that Zn^{2+} induces fluorescence changes by modulating the orbital energies of probe P-B (see more experimental details in Supplementary Information and Supplementary Table 1). As shown in Fig. 5c, for probe P-B, HOMO and LUMO energy levels of probe P-B, along with their energy gap (ΔE), were determined to be −5.09 eV, −1.99 eV, and 3.10 eV, respectively. These values indicate that probe P-B possesses a stable electronic structure with delocalized π-bonds, making excitation from the ground state relatively difficult. Upon complexation of probe P-B with Zn^{2+}, the HOMO and LUMO energy levels decreased to −6.20 eV and − 5.68 eV, respectively, with the energy gap narrowing to 0.52 eV. Consequently, the probe P-B-Zn^{2+} complex exhibits enhanced excitability due to this reduced energy gap. Based on the above results, the mechanism of P-B response to Zn^{2+} could be successfully explained, and the proposed identification mechanism was shown in Fig. 5d[60].

To explore the practical applicability of P-B as a fluorescent probe, we studied its application in the detection of Zn^{2+} in water and soil, respectively. Firstly, the standard addition recovery method was used to evaluate the feasibility of detecting Zn^{2+} in actual water samples. The water samples (from Laboratory tap and Fangming lake, Putian university, China) were spiked with different concentrations of Zn^{2+} and then the maximum fluorescence intensity was recorded. The linear equation between fluorescence intensity and the concentration of Zn^{2+} was used to calculate the detected concentration. As shown in Supplementary Table 4, the recovery rate and RSD of this method when detecting Zn^{2+} in tap water were in the ranges of 101.60% – 121.18% and 0.23% – 1.62%. While, the ranges of recovery rate and relative standard deviation for detecting Zn^{2+} in Fangming lake water were 100.08% – 111.47% and 0.80% – 1.87%. It is obvious that the concentration of Zn^{2+} obtained by this method is in good agreement with the added value, indicating that P-B has a good detection effect on Zn^{2+}, and can be used for quantitative detection in environmental water. Then, we applied P-B to the detection of Zn^{2+} in soil. As shown in Fig. 6a, the soil samples exhibit almost no fluorescence in the absence of the probe solution. However, after spraying with the probe solution, the soil emit bright yellowish green fluorescence. Based on the differences in fluorescence intensity, a rapid preliminary screening of Zn^{2+} contamination levels can be achieved. These results indicate that the probe has the potential to serve as a tool for on-site preliminary screening of soil Zn^{2+} contamination. It does not rely on complex instruments, and features portability and high efficiency, thus holding significant application value in environmental monitoring practices.

Subsequently, we investigated the application of P-B in data encryption and decryption based on its Zn^{2+}-responsive property. As shown in Fig. 6b, the word "LOVE" was written on filter paper using a Zn^{2+} solution. After natural air-drying, the "LOVE" disappeared. However, when sprayed with the probe solution, distinct yellowish-green markings matching the original content became clearly visible under ultraviolet light. Taking advantage of this "invisible-to-visible" transformation property, the probe P-B exhibits significant potential for applications in fields such as anti-counterfeiting, secure information storage, and encryption.

Fluorescence response of P-B to HClO

Similarly, the selectivity of probe P-B toward Cl^-, CH_3COO^-, NO^{2-}, NO^{3-}, SO_4^{2-}, SO_3^{2-} and HClO was investigated. When HClO was added to the P-B solution, the fluorescence intensities at both 500 nm and 600 nm

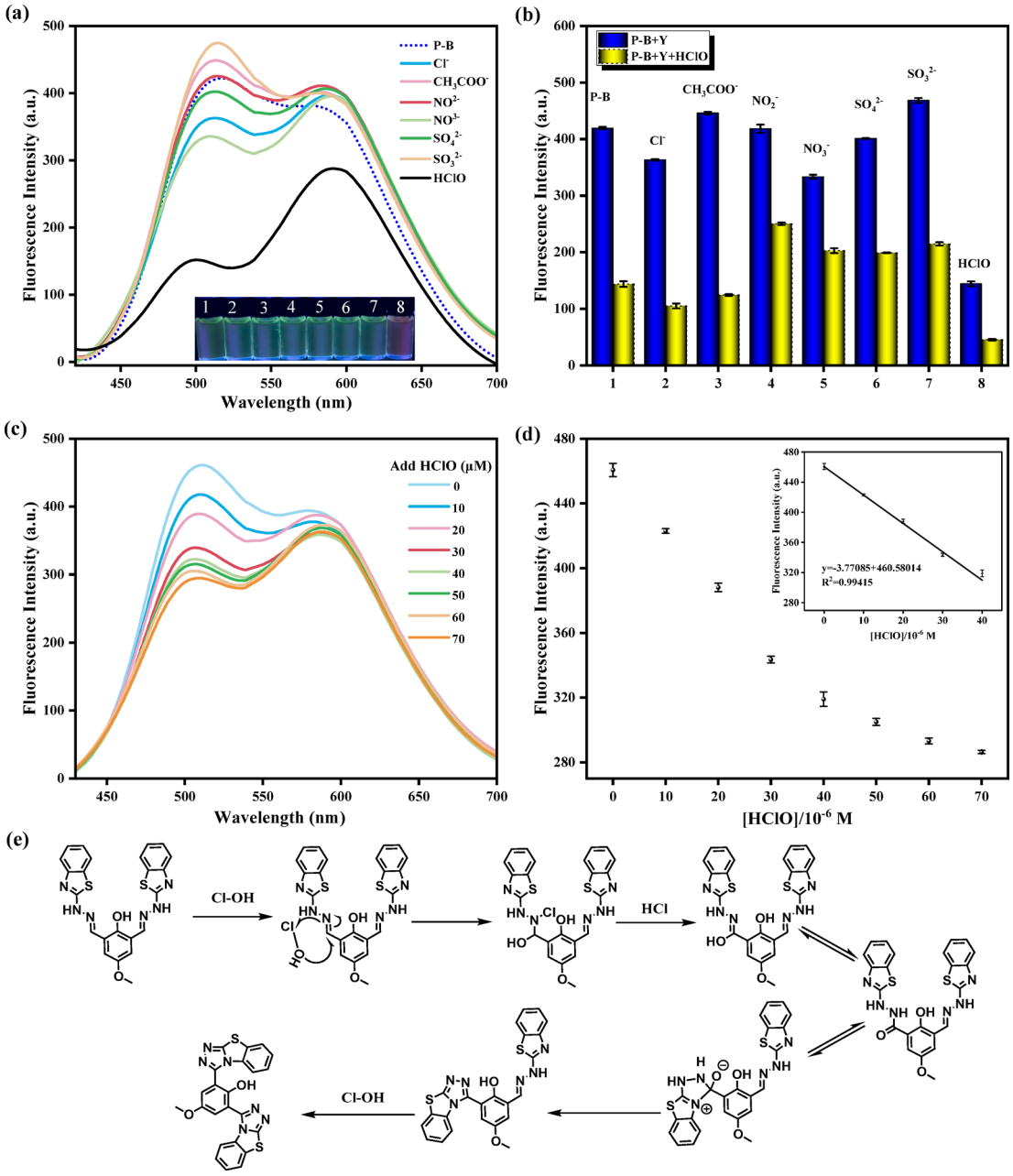

Fig. 7. (**a**) Fluorescence spectra of P-B in a DMSO/pure water in the presence of Cl^-, CH_3COO^-, NO_2^-, NO_3^-, SO_4^{2-}, SO_3^{2-}, and HClO. Inset:1-P-B, 2-Cl^-, 3-CH_3COO^-, 4-NO_2^-, 5-NO_3^-, 6-SO_4^{2-}, 7-SO_3^{2-}, 8- HClO. (**b**) Fluorescence intensities at 500 nm of P-B with various interfering ions in the absence of HClO (blue bars) or the presence of HClO (yellow bars). 1- P-B, 2- Cl^-, 3-CH_3COO^-, 4-NO^{2-}, 5-NO^{3-}, 6-SO_4^{2-}, 7- SO_3^{2-}, 8-HClO. (**c**) Fluorescence spectra of P-B with different concentration of HClO (0–70 μM). (**d**) Relationship between concentration of HClO and fluorescence intensity at 500 nm. (**e**) Recognition mechanism of the probe P-B for HClO. (DMSO/H_2O = 7/3, v/v, λ_{ex} = 400 nm, slits: 10 nm/10 nm).

decreased. However, no significant changes were observed in the fluorescence spectra upon the addition of other analytes (Fig. 7a). This indicated that P-B exhibits a specific response property to HClO. Then, we evaluated the anti-interference capability of P-B during the recognition process (Fig. 7b). The results showed that P-B not only exhibits strong anti-interference capability in hypochlorous acid (HClO) detection, but also possesses excellent selectivity and anti-interference performance for HClO detection.

The absolute slope of the linear relationship between the fluorescence intensity at 500 nm of P-B (10 μM) and HClO (0–70 μM), measured by the continuous titration method, was found to be 3.77085 (Fig. 7c and d). The standard deviation of fluorescence intensity at 500 nm for the 8 blank specimens was calculated as 0.30564 (Supplementary Fig. 10 and Supplementary Table 4). The calculated limit of detection (LOD) using the formula 3σ/k was 0.24 μM. Besides, a linear Stern-Volmer plot was obtained (Supplementary Fig. 2), and the bimolecular

quenching constant K_q and Stern-Volmner quenching constant K_{SV} was further calculated based on this plot. The measured bimolecular quenching constant K_q (5.48×10^{12} $M^{-1}s^{-1}$) was far higher than the diffusion-controlled limit (10^{10} $M^{-1}s^{-1}$), which proved that the probe quenching was not caused by diffusion collision. Instead, it is a static quenching process where the probe forms a complex with HClO, and the quenching is achieved through non-radiative transition[61,62]. Therefore, the binding constant K_a was approximately equal to Ksv, with a value of 0.945×10^4 M^{-1}.

To evaluate the sensitivity and stability of the probe in detecting HClO, we conducted fluorescence spectroscopy analysis at various incubation durations (Supplementary Fig. 11). The fluorescence intensity of P-B at 500 nm exhibited a rapid decline within the first 30 s, followed by a gradual leveling off, and stabilization within 40 min. In brief, the probe P-B demonstrated rapid responsiveness and good anti-interference ability in the detection of HClO. Since 2-(2-benzothiazolyl) hydrazone is a classic recognition site for detecting HClO, we hypothesized that the mechanism of P-B responding to HClO was as shown in the Fig. 7e. In the presence of HClO, the hydrazone and benzothiazole ring undergo a cyclization reaction to form a triazole, thereby quenching the fluorescence of the keto form of P-B[59,63,64].

Conclusion

In this study, we have successfully designed and synthesized a novel, dual-responsive bis-Schiff base fluorescent probe, P-B, through a straightforward synthetic route. This probe exhibits remarkable and distinct sensing capabilities for two environmentally and biologically significant analytes, Zn^{2+} and HClO. The detection of Zn^{2+} is achieved through the manifestation of a highly selective and sensitive "turn-on" fluorescence response at 520 nm by P-B. This phenomenon is driven by a Chelation-Enhanced Fluorescence (CHEF) mechanism. This response is characterized by its rapid kinetics (< 60 s), excellent anti-interference properties, and an impressively low limit of detection of 17.50 nM. In addition, the P-B probe possesses a unique "turn-off" sensing pathway for HClO, functioning through an irreversible oxidative cyclization reaction that effectively quenches its fluorescence. This configuration enables the selective detection of HClO, with an ultralow limit of detection of 0.24 μM and a rapid response time. The probe's dual functionality, which facilitates the detection of metal ions and reactive oxygen species through opposing fluorescence signals, underscores the versatility of its Schiff base scaffold.

The practical utility of this advanced molecular tool was successfully demonstrated through its application in complex real-world scenarios. P-B demonstrated efficacy in the expeditious, on-site preliminary screening of Zn^{2+} contamination in soil samples and in quantitative analysis of water samples. These findings underscore its considerable potential in environmental monitoring. Furthermore, its distinctive capacity to undergo a "transformation from invisible to visible" upon interaction with Zn^{2+} was ingeniously employed to develop a sophisticated information encryption and anti-counterfeiting system.

Data availability All data generated or analysed during this study are included in this published article and its Supplementary Information files.

Received: 16 August 2025; Accepted: 30 October 2025
Published online: 28 November 2025

References

1. Fang, L. & Watkinson, M. Subcellular localised small molecule fluorescent probes to image mobile Zn^{2+}. *Chem. Sci.* **11**, 11366–11379 (2020).
2. Du, C. et al. Diketopyrrolopyrrole-based fluorescence probes for the imaging of lysosomal Zn^{2+} and identification of prostate cancer in human tissue. *Chem. Sci.* **10**, 5699–5704 (2019).
3. Wang, Y. et al. Enhancing cancer treatment via Zn^{2+} interference with Zn-based nanomaterials. *Coord. Chem. Rev.* **500**, 215535 (2024).
4. Chen, Y. et al. Photoluminescence imaging of Zn^{2+} in living systems. *Chem. Soc. Rev.* **44**, 4517–4546 (2015).
5. Fan, D. et al. A Dual-Ion synergistic catalysis utilizing Zn^{2+}-regulated CdS_ySe_{1-y} ECL immunosensor employed for the ultrasensitive CA19-9 detection. *Anal. Chem.* **96**, 19750–19757 (2024).
6. Molina-López, J., Boschloo, G., Sun, L., Kloo, L. & Pettersson, H. Nutritional and methodological perspectives of zinc ions and complexes-physiological and pathological states. *Int. J. Electrochem. Sci.* **11**, 4470–4496 (2016).
7. Rahimzadeh, M. R. et al. Zinc poisoning-symptoms, causes, treatments. *Mini-Rev Med. Chem.* **20**, 1489–1498 (2020).
8. Kumar, N. et al. Design of highly selective Zn-coordinated polyampholyte for cancer treatment and inhibition of tumor metastasis. *Biomacromolecules* **25**, 1481–1490 (2024).
9. Yin, Y. et al. A potent nano-strategy for dual energy deprivation to inhibit pancreatic cancer progression. *Nano Today*. **59**, 102528 (2024).
10. Munir, T. et al. Fabrication of zinc doped titanium dioxide nanoparticles to inhibit Escherichia coli growth and proliferation of liver cancer cells (HepG2). *ACS Omega*. **9**, 34841–34847 (2024).
11. Chen, S. et al. Dual-channel versatile molecular sensing platform for individual and successive HClO and H_2S detection: applicable in toxic alerts of environmental samples and living organisms. *J. Hazard. Mater.* **465**, 133253 (2024).
12. Cheng, W., Boschloo, G., Sun, L., Kloo, L. & Pettersson, H. Individual and successive detection of H_2S and HClO in living cells and zebrafish by a dual-channel fluorescent probe with longer emission wavelength. *Anal. Chim. Acta.* **1156**, 338362 (2021).
13. Harrison, J. E. & Schultz, J. Studies on the chlorinating activity of myeloperoxidase. *J. Biol. Chem.* **251**, 1371–1374 (1976).
14. Zhan, Y. et al. Activatable NIR-II lanthanides-polymetallic oxomolybdate hybrid nanosensors for monitoring chemotherapy induced enteritis. *Adv. Funct. Mater.* **33**, 2301683 (2023).
15. Liang, Y. et al. A NIR BODIPY-based ratiometric fluorescent probe for HClO detection with high selectivity and sensitivity in real water samples and living zebrafish. *Spectrochim Acta Part. A: Mol. Biomol. Spectrosc*. **290**, 122268 (2023).
16. Yin, H. et al. Development of a new water-soluble fluorescence probe for hypochlorous acid detection in drinking water. *Food Chem. Mol. Sci.* **2**, 100027 (2021).
17. Li, S. et al. An endoplasmic reticulum-targeted near-infrared probe for monitoring HClO fluctuation in diabetic mice and human blood. *Sensor. Actuat B-Chem*. **379**, 133253 (2023).

18. Xu, X., Ding, H., Zhang, Q., Liu, G. & Pu, S. A ratiometric fluorescent probe with an extremely large emission shift for detecting ClO^- and its application in test strips and cell imaging. *Dyes Pigm.* **207**, 110776 (2022).
19. Świerczyńska, M. et al. Selective, stoichiometric and fast-response fluorescent probe based on 7-nitrobenz-2-oxa-1, 3-diazole fluorophore for hypochlorous acid detection. *Dyes Pigm.* **193**, 109563 (2021).
20. Li, Q. et al. Rapid-response near-infrared fluorescence probe for colorimetric detection of HClO and its applications in environmental monitoring and biological imaging. *Spectrochim Acta Part. A*. **320**, 124613 (2024).
21. Lan, Y. et al. Polysiloxane-based hyperbranched fluorescent probe for dynamic visualization of HClO in lysosomes and vivo. *Spectrochim Acta Part. A*. **294**, 122527 (2023).
22. Mao, G. J. et al. A lysosome-targetable two-photon excited near-infrared fluorescent probe for visualizing hypochlorous acid-involved arthritis and its treatment. *Spectrochim Acta Part. A*. **249**, 119326 (2021).
23. Shahbaz, M. et al. Recent advances in the fluorimetric and colorimetric detection of cobalt ions. *RSC Adv.* **14**, 9819–9847 (2024).
24. Xing, P. et al. Water solubility is essential for fluorescent probes to image hypochlorous acid in live cells. *Chem. Commun.* **54**, 9889–9892 (2018).
25. Shi, D., Chen, S. & Dong, B. Evaluation of HOCl-generating anticancer agents by an ultrasensitive dual-mode fluorescent probe. *Chem. Sci.* **10**, 3715–3722 (2019).
26. Tang, C., Wang, M., Wu, C. & Zheng, Q. Selective visualization of nitric oxide in living cells and tissue slices using a mitochondria-targetable fluorescent probe. *Dyes Pigm.* **217**, 111443 (2023).
27. Maiti, D., Islam, A. S. M., Sasmal, M., Prodhan, C. & Ali, M. Selective sensing of nitric oxide by 9,10-phenanthroquinonepyridoxal based fluorophore. *Photochem. Photobiol Sci.* **17**, 1213–1221 (2018).
28. Musameh, M. M. et al. Silk provides a new avenue for third generation biosensors: Sensitive, selective and stable electrochemical detection of nitric oxide. *Biosens. Bioelectron.* **103**, 26–31 (2018).
29. Adarsh, N., Krishnan, M. S. & Ramaiah, D. Sensitive naked eye detection of hydrogen sulfide and nitric oxide by Aza-BODIPY dyes in aqueous medium. *Anal. Chem.* **86**, 9335–9342 (2014).
30. Shen, R. & Qian, Y. A efficient light-controlled nitric oxide releaser in aqueous solution and its red fluorescence imaging in lysosome. *Dyes Pigm.* **176**, 108247 (2020).
31. Deshmukh, P. P., Navalkar, A., Maji, S. K. & Manjare, S. T. Phenylselenyl containing turn-on dibodipy probe for selective detection of superoxide in mammalian breast cancer cell line. *Sens. Actuat B-Chem.* **281**, 8–13 (2019).
32. Guo, R. Y. et al. Bioinspired design of reversible fluorescent probes for tracking nitric oxide dynamics in live cells. *CCS Chem.* **3**, 116–128 (2021).
33. Yang, M., Fan, J., Du, J. & Peng, X. Small-molecule fluorescent probes for imaging gaseous signaling molecules: current progress and future implications. *Chem. Sci.* **11**, 5127–5141 (2020).
34. Xu, Z. et al. Recent advances in formaldehyde-responsive fluorescent probes. *Chin. Chem. Lett.* **28**, 1935–1942 (2017).
35. Wu, D. et al. Naphthalimide-modified near-infrared cyanine dye with a large stokes shift and its application in bioimaging. *Chin. Chem. Lett.* **28**, 1979–1982 (2017).
36. Kumar, G. G. V. et al. Indole-derived multi-ion chemosensor for turn-on fluorescence and bio-imaging detection of Zn^{2+}, Al^{3+}, and Fe^{3+} ions. *J. Environ. Chem. Eng.* **13**, 117828 (2025).
37. Kumar, G. G. V. et al. A highly selective indole-based sensor for Zn^{2+}, Cu 2+, and al 3 + ions with multifunctional applications. *J. Mater. Chem. B*. **13**, 7335–7348 (2025).
38. Kumar, G. G. V. et al. Dual function Schiff-base as a selective fluorescence turn-on sensor for Zn^{2+} and a colorimetric sensor for Cu^{2+} and Fe^{3+} ions. *J. Photoch Photobiol A*. **454**, 115739 (2024).
39. Tamizhselvi, R. et al. Dual-channel fluorescent probe utilizing hydrazone for Zn^{2+} and Hg^{2+} detection: exploring distinct signaling mechanisms and applications in bioimaging and latent fingerprint analysis. *J. Photoch Photobiol A*. **452**, 115609 (2024).
40. Zavalishin, M. N., Pogonin, A. E. & Gamov, G. A. (eds) Hrgs2+-induced hydrolysis of fluorescein hydrazone: A new fluorescence probe for selective recognition Hg^{2+} in an aqueous solution. *J. Mol. Struct*. **1334**, 141930 (2025).
41. Zavalishin, M. N. et al. Synthesis and characterization of a vitamin B6-tetrazole hydrazone as a fluorescence probe for selective detection of Cd^{2+} and Ga^{3+} ions. *Opt. Mater.* **158**, 116493 (2025).
42. Zavalishin, M. N. et al. Pyridoxal 5′-phosphate 2-methyl-3-furoylhydrazone as a selective sensor for Zn^{2+} ions in water and drug samples. *J. Photochem. Photobiol A: Chem.* **432**, 114112 (2022).
43. Yan, L. et al. A near infrared fluorescent probe for detection and bioimaging of zinc ions and hypochlorous acid. *Anal. Chim. Actam*. **1206**, 339750 (2022).
44. So, H. et al. Detection of zinc (II) and hypochlorite by a thiourea-based chemosensor via two emission channels and its application in vivo. *Microchem J.* **155**, 104788 (2020).
45. Maity, S. et al. Dual-mode chemosensor for the fluorescence detection of zinc and hypochlorite on a fluorescein backbone and its cell-imaging applications. *Anal. Methods*. **14**, 2739–2744 (2022).
46. Zhang, Z. et al. A nanosensor made of sulfur–nitrogen co-doped carbon dots for off–on sensing of hypochlorous acid and Zn (II) and its bioimaging properties. *New. J. Chem.* **42**, 15895–15904 (2018).
47. Antony, R., Arun, T. & Manickam, S. T. D. A review on applications of chitosan-based schiff bases. *Int. J. Biol. Macromol.* **129**, 615–633 (2019).
48. Naik, K. H. K., Selvaraj, S. & Naik, N. Metal complexes of ONO donor schiff base ligand as a new class of bioactive compounds: synthesis, characterization and biological evolution. *Spectrochim Acta Part. Mol. Biomol. Spectrosc.* **131**, 599–605 (2014).
49. Tsantis, S. T., Tzimopoulos, D. I., Holynska, M. & Perlepes, S. P. Oligonuclear actinoid complexes with schiff bases as ligands-older achievements and recent progress. *Int. J. Mol. Sci.* **21**, 555 (2020).
50. Ceyhan, G. et al. Antioxidant, electrochemical, thermal, antimicrobial and alkane oxidation properties of tridentate schiff base ligands and their metal complexes. *Spectrochim Acta Part. Mol. Biomol. Spectrosc.* **81**, 184–198 (2011).
51. Pan, S. et al. A novel dual channel fluorescent probe for Ca^{2+} and Zn^{2+} based on a coumarin schiff base. *Chin. J. Chem.* **35**, 1263–1269 (2017).
52. Wang, J. et al. Schiff base aggregation-induced emission luminogens for sensing applications: a review. *ACS Sens.* **7**, 2521–2536 (2022).
53. Kumari, N. et al. Schiff bases: a versatile fluorescence probe in sensing cations. *J. Fluoresc*. **33**, 859–893 (2023).
54. Pan, X., Jiang, J., Li, J., Wu, W. & Zhang, J. Theoretical design of near-infrared Al3 + fluorescent probes based on salicylaldehyde acylhydrazone schiff base derivatives. *Inorg. Chem.* **58**, 12618–12627 (2019).
55. Li, C. et al. Reaction-based highly selective and sensitive monomer/polymer probes with schiff base groups for the detection of Hg^{2+} and Fe^{3+} ions. *Spectrochim Acta Part. Mol. Biomol. Spectrosc.* **243**, 118763 (2020).
56. Zhang, Q. et al. A schiff base dual mode turn-on fluorescent probe for selective detection of $HClO/ClO^-$ in buffer. *J. Mol. Struct.* **1343**, 142876 (2025).
57. Wang, K. et al. A coumarin Schiff's base two-photon fluorescent probe for hypochlorite in living cells and zebrafish. *RSC Adv.* **8**, 6904–6909 (2018).
58. Zhu, Y. et al. A highly sensitive turn-on fluorescent probe for real-time detecting hypochlorite and its application in living cells. *Talanta* **209**, 120548 (2020).
59. Lu, C. X. et al. A novel multifunctional fluorescent probe with ESIPT and AIE effects for the detection of Co^{2+} and HClO. *RSC Adv.* **15**, 4000–4013 (2025).

60. Li, L., Zhao, J. & Lü, C. W. ESIPT performance bis schiff base for multifunctional detection of Pb^{2+}, Mg^{2+} and Al^{3+} ions through turn on response and its biological application. *Res. Chem. Intermed.* **50**, 5017–5038 (2024).
61. Jayaraman, S. & Verkman, A. S. Quenching mechanism of quinolinium-type chloride-sensitive fluorescent indicators. *Biophys. Chem.* **85**, 49–57 (2000).
62. Lakowicz, J. R. & Weber, G. Quenching of fluorescence by oxygen. Probe for structural fluctuations in macromolecules. *Biochemistry* **12**, 4161–4170 (1973).
63. Wang, K. et al. A ratiometric benzothiazole-based fluorescence probe for selectively recognizing HClO and its practical applications. *Chin. Chem. Lett.* **31**, 2955–2959 (2020).
64. Wildes, P. D. & White, E. H. Dioxetane-sensitized chemiluminescence of lanthanide chelates. Chemical source of monochromatic light. *J. Am. Chem. Soc.* **93**, 6286–6288 (1971).

Acknowledgements

This work is supported by the National Natural Science Foundation of China (22405143), Natural Science Foundation of Fujian Province (2024J08220, 2024J01883), the Education and Research Project of Young and Middle-aged Teachers of Fujian Province (JAT220302), the Startup Fund for Advanced Talents of Putian University (2022054, 2024042), Cross-disciplinary Research Fund of Medical Engineering of Putian University (2024033), Natural Science Foundation of Inner Mongolia (2025QN02041), National Innovation and Entrepreneurship Training Program for College Students (202411498001X).

Author contributions

F. Y. and J. H. conceived the concept and supervised the research. Y. L. and Y. L. performed the experimental work. H. X. and X. P. provided experimental suggestions. All authors designed the experiments, analyzed the data, and drafted the manuscript.

Funding

This work is supported by the National Natural Science Foundation of China (22405143), Natural Science Foundation of Fujian Province (2024J08220, 2024J01883), the Education and Research Project of Young and Middle-aged Teachers of Fujian Province (JAT220302), Science and Technology Plan Project of Putian (2025GJJ005), the Startup Fund for Advanced Talents of Putian University (2022054, 2024042), Cross-disciplinary Research Fund of Medical Engineering of Putian University (2024033), Natural Science Foundation of Inner Mongolia (2025QN02041), National Innovation and Entrepreneurship Training Program for College Students (202411498001X).

Declarations

Competing interests

The authors declare no competing interests.

Additional information

Supplementary Information The online version contains supplementary material available at https://doi.org/10.1038/s41598-025-26717-3.

Correspondence and requests for materials should be addressed to X.L. or J.H.